# Conditional simulations of transient water-oil flow in randomly heterogeneous porous media

Mingjie Chen, Zhiming Lu, and George A. Zyvoloski

Hydrology, Geochemistry, and Geology Group (EES-6), Los Alamos National Laboratory, Los Alamos, New Mexico, USA.

## Abstract

This study is an extension of the stochastic analysis of transient two-phase flow in randomly heterogeneous porous media (Chen et al., 2006), by incorporating direct measurements of the random soil properties. The log-transformed intrinsic permeability, soil pore size distribution parameter, and van Genuchten fitting parameter are treated as stochastic variables that are normally distributed with a separable exponential covariance model. These three conditional random variables with given measurements are decomposed via Karhunen-Loève decomposition. Combined with the conditional eigenvalues and eigenfunctions of random variables, we conduct a series of numerical simulations using stochastic transient water-oil flow model (Chen et al., 2006) based on the KLME approach to investigate how the number and location of measurement points, different random soil properties, as well as the correlation length of the random soil properties, affect the stochastic behavior of water and oil flow in heterogeneous porous media.

Keywords: Karhunen-Loève decomposition; Conditional simulation; Water-oil flow; Uncertainty; Heterogeneity; NAPL; Porous media

## 1. Introduction

Many hazardous organic materials, such as oils, gasoline, and petrochemicals are widely used in the chemical and petroleum industry. Accidental release of these nonaqueous phase liquids (NAPL) to the subsurface are inevitable and represent a significant threat to water supply and eco-systems. Although the solubility of NAPL is low in water, but the concentration can still exceed drinking water standard a lot. Thus, small amount of NAPL can contaminate large volumes of groundwater over long period of time. Therefore, it is very important to understand the processes associated with contaminant migration and fate. Numerical multiphase flow models are used to study the various aspects of these processes in order to conduct risk assessment and design of cost-efficient remediation (e.g. Abriola, 1989). Another primary application of multiple fluid systems is petroleum reservoir engineering, which depends on the understanding of reservoir mechanics to design schemes for efficient oil recovery. A petroleum reservoir is a complicated mixture of porous rock, brine, hydrocarbon fluids. The structure of the

void space is tortuous and heterogeneous, which influence and even dominate the fluids flow. Full characterization of subsurface zone properties is a mission impossible. Many researchers resort to stochastic modeling of subsurface flow in the last two decades (Dagan, 1989; Gelhar, 1993; Zhang, 2002). This approach regards hydrological variables uncertain and treats them random, which define flow model in a stochastic context rather than in the traditional deterministic framework, and predict the output in terms of moments.

Zhang and Lu (2004) proposed a new stochastic approach, called KLME, based on Karhunen- Loève decomposition and polynomial expansions and applied it in saturated flow. Yang et al. (2004) extended KLME to analysis of saturated-unsaturated flow described by Richard's equation. Chen et al. (2005, 2006) developed stochastic multiphase flow model following the same approach. These studies demonstrated the accuracy and efficiency of KLME over traditional Monte-Carlo simulation or other stochastic approaches, however, the errors of moments resulted from KLME becomes severe when the variances of input variables are large. Many studies in conditional simulation indicate that conditioning on measurements of the log hydraulic conductivity can reduce the overall uncertainty of the log hydraulic conductivity, especially in the vicinity of the conditioning points, which may reduce the predictive uncertainties of flow and transport (Dagan, 1982; Guadagnini and Neuman, 1999a, 1999b; Lu et al., 2002; Tartakovsky, Neuman, and Lu, 1999). Therefore, conditional simulation will enable KLME to be applied effectively in flow system with drastic heterogeneous field, and more accurate in normal heterogeneous soil. Lu and Zhang (2004) conducted conditional simulations of saturated flow using KLME by incorporating measurements of the log hydraulic conductivity. The key step is to derive and calculate the conditional eigenvalues and eigenfuctions through unconditional ones of log hydraulic conductivity covariance function using kriging techniques. Running the stochastic KLME saturated flow model with these conditional eigenvalues and eigenfuctions leads to the conditional simulations. In this study, we extend their work from the saturated flow to the transient water-oil flow system with three random input variables, including log intrinsic permeability $Y$, log pore size distribution $\beta$, and log van Genuchten fitting parameter $\overline{n}$, with measurements in specific locations. We design a series of scenarios simulated by the stochastic KLME flow model to examine how the location and number of measurements, and the correlation length of covariance of these three random input variables influence the magnitude and distribution of uncertainties of predictive variables.

## 2. KL decomposition of conditional random field

A short description of Karhunen-Loève (KL) decomposition of unconditional random field is given below for readers to better understand conditional case. The KL decomposition of a stochastic process $\alpha(\mathbf{x},\theta)$, is based on the spectral decomposition of the covariance function of $\alpha$, $C_\alpha(\mathbf{x},\mathbf{y})$, with a set of orthogonal polynomials (Karhunen, 1947; Loève, 1948). $\mathbf{x}$ and $\mathbf{y}$ are spatial locations, and the argument $\theta$ denotes the random nature of the corresponding quantity. $C_\alpha(\mathbf{x},\mathbf{y})$ is symmetrical and positive definite, whose eigenfunctions are mutually orthogonal and form a complete set spanning the function space to which $\alpha(\mathbf{x},\theta)$ belongs (Ghanem and Dham, 1998). The mean-

removed stochastic process $\alpha'(\mathbf{x},\theta)$ can be expanded as follows (Zhang and Lu, 2004; Chen et al., 2005):

$$\alpha'(\mathbf{x},\theta)=\sum_{n=1}^{\infty}\xi_n(\theta)\sqrt{\lambda_n}\phi_n(\mathbf{x}), \tag{1}$$

where, $\lambda_n$ and $\phi_n(\mathbf{x})$ are the eigenvalues and eigenfunctions of the covariance kernel, respectively. $\phi_n(\mathbf{x})$ are orthogonal and deterministic functions and form a complete set

$$\int_\Omega \phi_n(\mathbf{x})\phi_m(\mathbf{x})d\mathbf{x}=\delta_{nm}, \tag{2}$$

Eigenvalues and eigenfunctions can be solved from the Fredholm equation

$$\int_\Omega C_\alpha(\mathbf{x},\mathbf{y})\phi(\mathbf{x})d\mathbf{x}=\lambda\phi(\mathbf{y}), \tag{3}$$

where $\Omega$ denotes the spatial domain where $\alpha(\mathbf{x},\theta)$ is defined. As defined, $\{\xi_n(\theta)\}$ forms a set of orthogonal random variables, and has properties of $\langle\xi_n(\theta)\rangle=0$, and $\langle\xi_n(\theta)\xi_m(\theta)\rangle=\delta_{nm}$, where $\delta_{nm}$ is the Krönecker delta function. For separable exponential covariance function such as

$$C_\alpha(\mathbf{x},\mathbf{y})=\sigma_\alpha^2\exp\left(-\sum_i\frac{|x_i-y_i|}{\eta_i}\right), \tag{4}$$

where $\sigma_\alpha^2$ and $\eta_i$ is the variance and correlation length of $\alpha(\mathbf{x},\theta)$ in the *i*th direction, analytical solutions of eigenvalues and eigenfunctions can be obtained by combing one dimensional analytical solution in each direction. For the general case, the eigenvalues and eigenfunctions have to be solved numerically via Galerkin-type method (Ghanem and Spanos, 1991).

Assume $N\alpha$ measurements of $\alpha_1$, $\alpha_2$, … , $\alpha_{N\alpha}$ are located at $\mathbf{x}_1$, $\mathbf{x}_2$, … , $\mathbf{x}_{N\alpha}$, and we can obtain the conditional mean and variance of $\alpha(\mathbf{x})$ using the kriging method:

$$\langle\alpha(\mathbf{x})\rangle^{(C)}=\langle\alpha(\mathbf{x})\rangle+\sum_{i=1}^{N\alpha}\mu_i(\mathbf{x})\left[\alpha(\mathbf{x}_i)-\langle\alpha(\mathbf{x}_i)\rangle\right], \tag{5}$$

$$C_\alpha^{(C)}(\mathbf{x},\mathbf{y})=C_\alpha(\mathbf{x},\mathbf{y})-\sum_{i,j=1}^{N\alpha}\mu_i(\mathbf{x})\mu_j(\mathbf{y})C_\alpha(\mathbf{x}_i,\mathbf{x}_j), \tag{6}$$

where, weighting coefficients $\mu_i(\mathbf{x})$ represent the relative significance of each measurement $\alpha(\mathbf{x}_i)$ in predicting the $\langle\alpha\rangle^{(C)}$ at location $\mathbf{x}$, and can be determined by the following equations:

$$\sum_{i=1}^{N\alpha}\mu_i(\mathbf{x})C_\alpha(\mathbf{x}_i,\mathbf{x}_j)=C_\alpha(\mathbf{x},\mathbf{x}_j),\ j=1,2,...,N\alpha. \tag{7}$$

Apparently, the two-point conditional covariance $C_\alpha^{(C)}(\mathbf{x},\mathbf{y})$ is no longer stationary, and depends on the locations of $\mathbf{x}$ and $\mathbf{y}$, instead of their separation distance. Generally, the corresponding eigenvalues $\lambda_n^{(C)}$ and eigenfunctions $\phi_n^{(C)}$ have to be solved numerically (Ghanem and Spanos, 1991). However, for special case of a two-dimensional rectangular or three-dimensional brick domain, conditional eigenvalues and eigenfunctions can be related to their unconditional counterpart $\lambda_n$ and $\phi_n$, which can be obtained easily

(Zhang and Lu, 2004). The basic idea of this algorithm is to expand $\mu_i(\mathbf{x})$ and $\phi_n^{(C)}$ based on unconditional eigenfunctions $\phi_n$ as follows (Lu and Zhang, 2004):

$$\mu_i(\mathbf{x}) = \sum_{k=1}^{\infty} \mu_{ik}\phi_k(\mathbf{x}), \tag{8}$$

$$\phi^{(C)}(\mathbf{x}) = \sum_{k=1}^{\infty} d_k\phi_k(\mathbf{x}), \tag{9}$$

where $\mu_{ik}$, $d_k$ are coefficients determined by

$$\sum_{i=1}^{N\alpha} C_\alpha(\mathbf{x}_i, \mathbf{x}_j)\mu_{ik} = \lambda_k\phi_k(\mathbf{x}_j), j = 1,2,...,N\alpha; k = 1,2,..., \tag{10}$$

$$\lambda_k d_k - \sum_{m=1}^{\infty}\left(\sum_{i,j=1}^{N\alpha} C_\alpha(\mathbf{x}_i, \mathbf{x}_j)\mu_{im}\mu_{ik}\right)d_m = \lambda^{(C)}d_k, k = 1,2,... \quad . \tag{11}$$

The computational efforts of obtaining conditional eigenvalues and eigenfunctions in this way are much less than that of solving them numerically via Galerkin-type method. It should be noted that this algorithm is only applicable to special type of covariance model described above.

## 3. KL-based conditional moment equations

The governing equations for the transient water-oil phase flow can be written as (Abriola and Pinder, 1985):

$$\frac{\partial^2 P_l(\mathbf{x},t)}{\partial x_i^{\,2}} + \frac{\partial Z_l(\mathbf{x},t)}{\partial x_i}\left[\frac{\partial P_l(\mathbf{x},t)}{\partial x_i} + \rho_l g\delta_{i1}\right] = \exp\left[-Z_l(\mathbf{x},t)\right]\left[\phi\frac{\partial S_l(\mathbf{x},t)}{\partial t} - F_l(\mathbf{x},t)\right], \tag{12}$$

where $P_l(\mathbf{x},t)$ is the fluid pressure; $l$ denotes liquids ($l = w, o$); $S_l(\mathbf{x},t)$ are the water ($l = w$) and oil ($l = o$) saturations; $\mathbf{x}$ is the position vector in 2- or 3-D; $F_l(\mathbf{x},t)$ is a source or sink term; $Z_l(\mathbf{x},t) = \ln\lambda_l(\mathbf{x},t)$, and $\lambda_l(\mathbf{x},t) = k(\mathbf{x})k_{rl}(S_l)/\mu_l$ is liquid mobility, where $k(\mathbf{x})$ is the intrinsic permeability of porous media, $k_{rl}$ is the water or oil relative permeability, and $\mu_l$ is the liquid dynamic viscosity; $\rho_l$ is fluid density, and $\phi$ is the porosity of the media. $\delta_{i1}$ is the Krönecker delta function, which equals 1 when $i$ is 1 (upward direction) or 0 otherwise. The boundary conditions are as follows:

$$P_l(\mathbf{x},0) = P_{l0}(\mathbf{x}), \qquad \mathbf{x}\in\Omega, \tag{13}$$

$$P_l(\mathbf{x},t) = P_{lt}(\mathbf{x},t), \qquad \mathbf{x}\in\Gamma_D, \tag{14}$$

$$n_i(\mathbf{x})\exp\left[Z_l(\mathbf{x},t)\right]\left[\frac{\partial P_l(\mathbf{x},t)}{\partial x_i} + \rho_l g\delta_{i1}\right] = -Q_l(\mathbf{x},t),\ \mathbf{x}\in\Gamma_N, \tag{15}$$

where $P_{l0}(\mathbf{x})$ is the initial pressure in the domain $\Omega$; $P_{lt}(\mathbf{x},t)$ is the prescribed pressure on a Dirichlet boundary segment $\Gamma_D$; $Q_l(\mathbf{x},t)$ is the prescribed fluid flux across Neumann boundary segments $\Gamma_N$; $g$ is the gravity vector; $n(\mathbf{x})$ is the outward unit vector normal to the boundary $\Gamma_N$.

van Genuchten (1980) model is used to describe the relationship between saturation, capillary pressure and relative permeability.

$$k_{rw} = \overline{S}_w^{1/2}\left[1-\left(1-\overline{S}_w^{1/m}\right)^m\right]^2, \tag{16}$$

$$k_{ro} = \left(1-\overline{S}_w\right)^{1/2}\left(1-\overline{S}_w^{1/m}\right)^{2m}, \tag{17}$$

$$\overline{S}_w = \left[1+\left(\alpha P_c\right)^n\right]^{-m}, \tag{18}$$

where $\overline{S}_w = \left(S_w - S_{wr}\right)/\left(1-S_{wr}\right)$ is the effective water saturation, $S_w = 1-S_o$ is water saturation, and $S_{wr}$ is the residual water saturation, $\alpha$ is the pore size distribution, $P_c = P_o - P_w$ is the capillary pressure, $n$ is the van Genuchten fitting parameters and $m = 1-1/n$. In our study, log transformed intrinsic permeability, pore size distribution, and van Genuchten fitting parameters are considered random fields, and expanded using conditional KL decomposition described in the last section. The governing equations (12)-(15) are the stochastic water-oil flow model, and are solved via KL-based perturbation methods.

The mathematical formulation of the equations (12)-(15) using the KLME method are presented by Chen et al. (2006) in detail. Basically, the idea of the KLME approach is to decompose stochastic governing equations of flow into a series of deterministic equations, which can be solved using existing numerical techniques. The solutions are then assembled to obtain explicit and intelligible moments of the dependent variables. The KL-based conditional moment equations can be derived in the similar way. Zeroth order equations are shown as

$$\begin{aligned}&\frac{\partial^2 P_w^{(0)}(\mathbf{x},t)}{\partial x_i^{\,2}} + \frac{\partial Z_w^{(0)}(\mathbf{x},t)}{\partial x_i}\left[\frac{\partial P_w^{(0)}(\mathbf{x},t)}{\partial x_i} + \rho_w g \delta_{i1}\right] \\ &= \frac{C_{ow}^{(0)}(\mathbf{x},t)}{\exp\left[Z_w^{(0)}(\mathbf{x},t)\right]}\frac{\partial P_c^{(0)}(\mathbf{x},t)}{\partial t} - \frac{F_w(\mathbf{x},t)}{\exp\left[Z_w^{(0)}(\mathbf{x},t)\right]},\end{aligned} \tag{19}$$

$$\begin{aligned}&\frac{\partial^2 P_o^{(0)}(\mathbf{x},t)}{\partial x_i^{\,2}} + \frac{\partial Z_o^{(0)}(\mathbf{x},t)}{\partial x_i}\left[\frac{\partial P_o^{(0)}(\mathbf{x},t)}{\partial x_i} + \rho_o g \delta_{i1}\right] \\ &= \frac{-C_{ow}^{(0)}(\mathbf{x},t)}{\exp\left[Z_o^{(0)}(\mathbf{x},t)\right]}\frac{\partial P_c^{(0)}(\mathbf{x},t)}{\partial t} - \frac{F_o(\mathbf{x},t)}{\exp\left[Z_o^{(0)}(\mathbf{x},t)\right]},\end{aligned} \tag{20}$$

and first order equations are shown as

$$\frac{\partial^2 P_{w,n}^{(1)}(\mathbf{x},t)}{\partial x_i^{\,2}} + J_{wi}(\mathbf{x},t)\frac{\partial Z_{w,n}^{(1)}(\mathbf{x},t)}{\partial x_i} + \frac{\partial Z_w^{(0)}(\mathbf{x},t)}{\partial x_i}\frac{\partial P_{w,n}^{(1)}(\mathbf{x},t)}{\partial x_i}$$
$$= \frac{C_{ow}^{(0)}(\mathbf{x},t)}{\exp\left[Z_w^{(0)}(\mathbf{x},t)\right]}\left[\frac{\partial P_{c,n}^{(1)}(\mathbf{x},t)}{\partial t} - Z_{w,n}^{(1)}(\mathbf{x},t)\frac{\partial P_c^{(0)}(\mathbf{x},t)}{\partial t}\right] \tag{21}$$
$$+ \frac{C_{ow,n}^{(1)}(\mathbf{x},t)}{\exp\left[Z_w^{(0)}(\mathbf{x},t)\right]}\frac{\partial P_c^{(0)}(\mathbf{x},t)}{\partial t} - \frac{F_w(\mathbf{x},t)}{\exp\left[Z_w^{(0)}(\mathbf{x},t)\right]}Z_{w,n}^{(1)}(\mathbf{x},t),$$

$$\frac{\partial^2 P_{o,n}^{(1)}(\mathbf{x},t)}{\partial x_i^{\,2}} + J_{oi}(\mathbf{x},t)\frac{\partial Z_{o,n}^{(1)}(\mathbf{x},t)}{\partial x_i} + \frac{\partial Z_o^{(0)}(\mathbf{x},t)}{\partial x_i}\frac{\partial P_{o,n}^{(1)}(\mathbf{x},t)}{\partial x_i}$$
$$= \frac{-C_{ow}^{(0)}(\mathbf{x},t)}{\exp\left[Z_o^{(0)}(\mathbf{x},t)\right]}\left[\frac{\partial P_{c,n}^{(1)}(\mathbf{x},t)}{\partial t} - Z_{o,n}^{(1)}(\mathbf{x},t)\frac{\partial P_c^{(0)}(\mathbf{x},t)}{\partial t}\right] \tag{22}$$
$$- \frac{C_{ow,n}^{(1)}(\mathbf{x},t)}{\exp\left[Z_o^{(0)}(\mathbf{x},t)\right]}\frac{\partial P_c^{(0)}(\mathbf{x},t)}{\partial t} - \frac{F_o(\mathbf{x},t)}{\exp\left[Z_o^{(0)}(\mathbf{x},t)\right]}Z_{o,n}^{(1)}(\mathbf{x},t),$$

$C_{ow}(\mathbf{x},t)$ is a stochastic variable depending on the three random fields. There are one zeroth order equations, but *n* of first order equations. *n* is the terms needed to capture the most of uncertainty. Solve the series of equations, and we can construct mean and variance of fluid pressures.

$$\left\langle P_l(\mathbf{x},t)\right\rangle \approx \left\langle P_l^{(0)}(\mathbf{x},t)\right\rangle + \left\langle P_l^{(1)}(\mathbf{x},t)\right\rangle = P_l^{(0)}(\mathbf{x},t)\,, \tag{23}$$

$$C_{P_l}(\mathbf{x},\mathbf{y},t) = \sum_{n=1}^{\infty} P_{l,n}^{(1)}(\mathbf{x},t)P_{l,n}^{(1)}(\mathbf{y},t)\,. \tag{24}$$

The variances of fluid saturation can be found in the similar way. This stochastic KLME water-oil flow model was coded using Fortran.

## 4. Illustrative examples

In this section, we use the stochastic water-oil flow model to examine how input random fields and measurements influence stochastic behavior of fluid pressure and saturation. We don't conduct Monte-Carlo simulations for these cases in this study, since the accuracy and efficiency of the developed stochastic model have been demonstrated by Chen et al. (2006), and our goal is to use it to investigate the problems of interest.

We assume the log intrinsic permeability $Y(\mathrm{x})$, log pore-size distribution parameter $\beta(\mathrm{x})$, and log van Genuchten fitting parameter $\overline{n}(\mathbf{x})$ to be random fields with a separable exponential covariance functions as equation (4). We consider a two-dimensional domain in a water-oil flow system in heterogeneous porous medium. This vertical cross section is 3 m deep and 0.96 m wide, uniformly discretized into 50×16 square elements of 0.06 m × 0.06 m. The no-flow conditions are prescribed at two lateral boundaries. The water and oil pressure are specified at the bottom of the domain (Figure 1). Oil is leaked into the domain at node X1 = 2.4 m, X2 = 0.48 m (black solid circle in Figure 1) and a

constant precipitation rate is fixed at the top boundary. The soil porosity is 0.5. The initial water saturation around the oil leak point is above 0.98. The initial values and boundary conditions represent a continuous DNAPL leak into the nearly clean soil with constant precipitation on the soil surface.

The primary fluids properties, random soil properties, and boundary conditions for the baseline case are listed in Table 1. The measurements data are extracted from the "true" field, which can be generated from the unconditional Karhunen-Loève decomposition (Equation 1). Based on this unconditional simulation of baseline case, we will conduct conditional simulations with different number of random variables, measurements, and correlation length (Table 2). All the cases are simulated to 1 day.

### 4.1 Number of measurements

Case 1 is the conditional counterpart of the unconditional baseline case, with measurements of $Y(\mathbf{x})$, $\beta(\mathbf{x})$, and $\bar{n}(\mathbf{x})$ at the location of oil leak (0.48 m, 2.4 m), while Case 2 have additional three measurements at X1 = 1.8, 1.2, 0.6 m along the central vertical line. All the four measurement locations are denoted with small circle in Figure 1. To simulate conditional Case 1 and Case 2, we first solve for the unconditional eigenvalues and eigenfunctions, then compute conditional ones using the algorithm described in Section 2. The first 50 terms of unconditional and conditional eigenvalues and eigenfunctions of covariance of $\beta(\mathbf{x})$ are shown in Figure 2, where condition 1 has only one measurement at X1=2.4 m and condition 2 has all the four measurements. It is seen that conditional eigenvalues with four measurements is less than those with one measurement, which, in turn, are less than those of the unconditional eigenvalues. It indicates that variability of $\beta(\mathbf{x})$ in Case 2 are smaller than that in both Case 1 and unconditional baseline case. It is shown that the series of eigenvalues is monotonously decreasing and the first 50 terms can account for about 90% of the total variability. Figure 3 compares the third term of unconditional eigenfunctions, conditional eigenfunctions with one measurement (condition 1) and four measurements (condition 2). It is obvious that the measurements affect the characteristic values and scales of eigenfunction fields.

Figure 4 and Figure 5 show the conditional means and variances of $\beta(\mathbf{x})$ to be used in Case 1 and Case 2. The values of means around measurements are significantly influenced by the measurements. The variability decreases around the measurements in a radiated distribution, and the overall variability of $\beta(\mathbf{x})$ used in Case 2 is a little bit smaller than that used in Case 1, since Case 2 has all the four measurements honored in the random fields.

Figure 6 compares the water saturation variances simulated from Baseline Case, Case 1, and Case 2. For the unconditional case, the water saturation variance presents a radiated downward distribution around the oil leak location, indicating more uncertainty about the location of the oil as the oil migrates downwards (oil is denser than water). For the conditional cases (Case 1, 2), the conditioning effect is very localized, reducing the uncertainty of water saturation around the condition points. The variances of oil pressure and capillary pressure along central vertical line of the domain for the three cases are shown in Figure 7. It is seen that the peak of the profile for Baseline Case at the oil leak location are damped for Case 1 and 2, and the reduction of variability extends to low part of the domain for Case 2, since there are additional three measurements below the

measurement at the oil leak location. In addition, the overall oil and capillary pressure variability are reduced for the two conditional cases, compared to the unconditional case. The average variance of oil pressure across the profile is reduced relatively by 92.50% in Case 1, and 94.13% in Case 2 from Baseline Case, respectively. For capillary pressure, the figures are 93.21% and 93.50% respectively. That means more than 90% of the overall uncertainty of oil or capillary pressure along vertical central line is reduced. In addition to the number of measurements, the location of measurements is another factor influencing the reduction of uncertainty. As is shown in Figure 7, the measurement at oil leak location, where the prediction is most uncertain, contributes much more to the uncertainty reduction than the other three measurements.

We also examine the effect of the oil source term to the prediction uncertainty. We increase the oil injection rate from 100 kg/d in Baseline Case, Case 1 and 2 to 10000 kg/d in Baseline Case I, Case 3 and 4. The variances profile of oil pressure and capillary pressure are presented in Figure 8. The variances profile from the unconditional Baseline Case I, conditional Case 3 with one measurement, and Case 4 with four measurements show the same behavior as those in the low oil injection rate (Figure 7), but the magnitude of is almost 4 orders greater. It indicates that the strength of oil source term has the overwhelming effect on the magnitude of prediction variance over the uncertainty of soil properties, from which the prediction variability originate. The role of the former one in the prediction uncertainty is like amplifier, while the latter is the sound source.

### 4.2 Number of conditioned random field

All the three random fields are conditioned simultaneously at one or four locations in Case 1 to 4. In this section, we modify Case 3, and use unconditional $\overline{n}$, $\beta$, $Y$ field in Case 5, 6, 7 respectively, and leave the other two fields conditional (Table 2). By simulating these cases, we attempt to find the relative importance of the three random variables to the prediction uncertainty.

Figure 9(a) presents the variance profile of oil pressure along central vertical line of modeling domain for Case 3, 5, 6 and 7. With $\beta$ and $\overline{n}$ conditioned at the oil leak location, variances of oil pressure from Case 7 are smaller than those from unconditional Baseline Case I (Figure 8), but well above those from Case 3, in which all the three random variables $Y$, $\beta$, $\overline{n}$ are conditioned at the oil leak location. Compared to Case 5, in which $Y$, $\beta$ are conditioned, and Case 6, in which $Y$, $\overline{n}$ are conditioned, the reduction of oil pressure variability is the smallest in Case 7. It seems that the conditional $Y$ is more efficient in reducing uncertainty of oil pressure than $\beta$, $\overline{n}$. The difference between conditioned $\beta$ and $\overline{n}$ is not so large, although, the reduction of oil pressure variability with $\beta$ conditioned (Case 5) is more than that with $\overline{n}$ conditioned (Case 6).

The variances behavior around the oil leak location (X1 = 2.4m) present different characteristic between the cases in Figure 9(a). Case 7 is simulated with $\beta$, $\overline{n}$ conditioned at the oil leak location, but the oil pressure variances still peak at that point. With additional $Y$ conditioned in Case 3, oil pressure variances reach a recess at the oil leak location. In Case 5 and 6, with $Y$, $\beta$ and $Y$, $\overline{n}$ conditioned respectively, the peak of oil pressure variance profile along central vertical line in Case 7 and the recess in Case 3 at the oil leak location are flatten out. These behaviors indicate that the measurement of

$Y$ can reduce the oil pressure uncertainty a lot more than that of $\beta$ or $\overline{n}$ locally, and hence the overall oil pressure uncertainty throughout the modeling domain.

The behavior of capillary pressure variance profile is shown in Figure 9(b). Similar with oil pressure variance, Case 7 produces much larger capillary pressure variance than Case 3, 5, and 6, although it was smaller than unconditional case. In contrast to oil pressure variability, the capillary pressure variability reduces less in Case 5 than in Case 6. Also, the capillary pressure variability reaches the peak at the oil leak location in Case 7. However, the profile of capillary pressure variance in Case 5 and 6 arrives at a recess at the oil leak location, like Case 3. In addition, the variances of capillary pressure in Case 5 and 6 differ from Case 3 less than those of oil pressure in Figure 9(a), indicating the relative importance of uncertainty of intrinsic permeability $Y$ versus the pore size distribution $\beta$ or the van Genuchten fitting parameter $\overline{n}$ to the uncertainty of capillary pressure is bigger than the oil pressure.

### 4.3 Correlation length of random field

To examine the influence of correlation lengths of random soil properties, we conduct Baseline Case II and Case 8 with half correlation length of that in Baseline Case and Case 1 (Table 2). Figure 10 (a) shows us that the distribution of variances of water saturation for Baseline Case II is radial centered at oil leak location, similar to that for Baseline Case (Figure 6 a). Oil saturation variance can be proved to be the same as the water saturation variances in such a water-oil flow system. The magnitude of variance in Baseline Case II is slightly smaller than that in Baseline Case, since random fields with smaller correlation length reduce the prediction variability (Zhang and Lu, 2004). Another possible reason is because more terms needed in KL to capture the uncertainty of random fields with shorter correlation length. In Baseline Case II, we use the same number to terms as that in Baseline Case, so the finial assemble of variances are a little smaller. Similarly, the variability of water saturation from Case 8 (Figure 10 b) is a little smaller than that from Case 1 (Figure 6 b). Owing to the measurements of the three of soil random fields at the oil leak location, the variances fall substantially but very localized around the location.

What should be noted in the two figures is that the influencing region of the measurement at oil leak location in Case 1 is larger than that in Case 8, which is expected, since the larger correlation length indicated the larger affecting area of each conditioning point, which would reduce relatively the overall prediction variability more. The average relative reduction of oil and capillary pressure variability profile along central vertical line of conditional Case 1 from unconditional Baseline Case are 92.50% and 93.21% (Figure 7). The reductions of Case 8 from Baseline Case II are 91.29% and 90.58% (Figure 11), which are smaller than the counterpart with larger correlation length (Case 1 v.s. Baseline Case). The peaks of oil pressure and capillary pressure profiles at the oil leak location in Case 8 is obvious in Figure 11, while the peaks in Case 1 is almost damped in Figure 7. That demonstrate small correlation length of random input fields has small reduction of prediction uncertainty locally, in addition to the small influence area. Comparison between Figure 7 and Figure 11 indicates that there are few differences of oil and capillary pressure variability behavior other than that mentioned above.

## 5. Summary and Conclusions

In modeling subsurface multiphase flow, the hydrogeology properties characteristic of large heterogeneity lead to huge uncertainty of migration of flowing multiple fluids. How to reduce the uncertainty and make prediction as accurate as possible is the major concern for engineers to make NAPL pollution remediation and petroleum reservoir simulation. In this study, we manage to reduce the prediction variability by incorporating existing measurements of log intrinsic permeability, pore size distribution, and van Genuchten parameters into the unconditional KLME method for water-oil flow system developed earlier. The key idea of the algorithm is to compute the conditional covariance of the random soil properties via kriging method, and decompose the conditional covariance into the conditional eigenvalues and eigenfunctions. After solving a series of decomposed deterministic multiphase flow equations with these conditional eigenvalues and eigenfunctions, we can assemble prediction mean and variances (water, oil and capillary pressure; water and oil saturation). A series of cases were simulated to investigate how the random soil properties and measurements influence the stochastic behavior of predictions. The main findings of this paper are summarized as follows:

1. The conditional KLME method is applicable to stochastic analysis of transient water-oil flow in heterogeneous porous media, and provide a potential tool for remediation and petroleum reservoir engineers to better understand the multiphase flow in heterogeneous subsurface area, especially under such a situation that some field measurements are available.
2. The measurements can reduce the prediction variability in the neighboring area remarkably, as well as the overall prediction variability across the domain. More measurements, more reduction of variability. Some measurements in the key location (e.g. source term location) can reduce the uncertainty much more effectively.
3. In our study, the uncertainty of intrinsic permeability seems to contribute more to the uncertainty of prediction than the other two random variables do, while the conditional pore size distribution and van Genuchten parameter field only make the slight difference of uncertainty reduction of prediction. Thus, adding measurements to the random intrinsic permeability fields can reduce the prediction variability more than the other two random fields.
4. The increase of source term strength can increase the variances of prediction by several orders, and counteract the uncertainty reduction of conditioned random input variables many times. However, the source of prediction uncertainty is from the random input, the increase of source term strength only amplifies it.
5. Small correlation lengths of random fields can reduce the prediction variability. Also, more terms in KLME approach needed for smaller correlation length of random fields to capture the uncertainty of fluid flow. The smaller the correlation length, the smaller area of one measurement can influence, and the smaller the reduction of the uncertainty.

### Acknowledgement

The authors would like to acknowledge the funding from the oil shale project cooperated between Chevron Energy Technology Company and Los Alamos National Laboratory.

## References


Abriola, L. (1989), Modeling multiphase migration of organic chemicals in groundwater systems - A review and assessment, *Environmental Health Perspectives*, 83, 117-143.

Abriola, L. and G. Pinder (1985), A multiphase approach to the modeling of porous media contamination by organic compounds: 1: Equation development, *Water Resour. Res.*, 21(1), 11-18.

Chen, M., D. Zhang, A.A. Keller, and Z. Lu (2005), A stochastic analysis of steady state two-phase flow in heterogeneous media. *Water Resour. Res*., 41, w01006, doi:10.1029/2004WR003412.

Chen, M., A.A. Keller, D. Zhang, Z. Lu, and G.A. Zyvoloski (2006), A Stochastic analysis of transient two-phase flow in heterogeneous porous media, *Water Resour. Res*., 42, W03425, doi:10.1029/2005WR004257.

Dagan, G. (1982), Stochastic modeling of groundwater flow by unconditional and conditional probabilities: 1. Conditional simulation and the direct problem, *Water Resour. Res*., 18(4), 813-833.

Dagan, G. (1989), *Flow and Transport in Porous Formations*, Springer-Verlag, New York.

Ghanem, R. and S. Dham (1998), Stochastic Finite Element Analysis for Multiphase Flow in Heterogeneous Porous Media, *Transport in Porous Media*, 32, 239-262.

Ghanem, R. and D. Spanos (1991), *Stochastic Finite Elements: a Spectral Approach*, New York, Springer-Verlag.

Gelhar, W. (1993), *Stochastic Subsurface Hydrology*, Prentice-Hall, Englewood Cliffs, NJ.

Guadagnini, A., S.P. Neuman (1999a), Nonlocal and localized analyses of conditional mean steady-state flow in bounded, randomly nonuniform domains: 1. Theory and computational approach, *Water Resour. Res*., 35(10), 2999-3018.

Guadagnini, A., S.P. Neuman (1999b), Nonlocal and localized analyses of conditional mean steady-state flow in bounded, randomly nonuniform domains: 2. Computational examples, *Water Resour. Res*., 35(10), 3019-3039.

Karhunen, K. (1947), Uber lineare methoden in der wahrschein-lichkeitsrechnung. *Amer. Acad. Sci.*, Fennicade, Ser. A, I, Vol 37, 3-79, (Translation: RAND Corporation, Santa Monica, California, Rep. T-131, Aug. 1960).

Loeve, M. (1948), *Fonctions aleatorires du second ordre, supplement to P. Levy*. Processus Stochastic et Mouvement Brownien, Paris, Gauthier, Villars.

Lu, Z., S.P. Neuman, A. Guadagnini, and D.M. Tartakovsky (2002), Conditional moment analysis of steady state unsaturated flow in bounded, randomly heterogeneous soils, *Water Resour. Res*., 38(4), 10.1029/2001WR000278.

Lu, Z and D. Zhang (2004), Conditional simulations of flow in randomly heterogeneous porous media using a KL-based moment-equation approach, *Advances in Water Resources*, 27, 859-874.

Tartakovsky, D.M., S.P. Neuman, and Z. Lu (1999), Conditional stochastic averaging of steady state unsaturated flow by means of Kirchhoff transformation, *Water Resours. Res*., 35(3), 731-745.

van Genuchten, M. (1980), A closed form solution for predicting the hydraulic conductivity of unsaturated soils*, Soil Sci. Soc. Am. J*. 44, 892-898.

Yang, J., D. Zhang, and Z. Lu (2004), Stochastic analysis of saturated-unsaturated flow in heterogeneous media by combing Karhunene-Loeve expansion and perturbation method. *J. Hydrology*, 29, 418-38

Zhang, D. (2002), *Stochastic Methods for Flow in Porous Media: Coping with Uncertainties*, Academic Press, San Diego, Calif., ISBN 012-7796215.

Zhang, D., and Z. Lu (2004), Evaluation of Higher-Order Moments for Saturated Flow in Randomly Heterogeneous Media via Karhunen-Loeve Decomposition, *Journal of Computational Physics*, 194(2), 773-794.

## Tables and Figures

**Table 1. Soil and fluid properties and boundary conditions**

| Parameter name | Symbol | Units | Baseline Case |
|---|---|---|---|
| Water density | $\rho_w$ | kg/m$^3$ | 997.81 |
| Oil density | $\rho_o$ | kg/m$^3$ | 1500 |
| Water viscosity | $\mu_w$ | Pa·s | 1.0x10$^{-3}$ |
| Oil viscosity | $\mu_o$ | Pa·s | 6.5x10$^{-4}$ |
| Mean intrinsic permeability | $<k>$ | m$^2$ | 3.78x10$^{-11}$ |
| Mean pore size distribution | $<\alpha>$ | 1/Pa | 1.23x10$^{-4}$ |
| Mean fitting parameter n | $<n>$ | - | 1.35 |
| Variance of permeability | $\sigma_k^2$ | - | 5.20x10$^{-22}$ |
| Variance of pore size distribution | $\sigma_\alpha^2$ | - | 1.55x10$^{-10}$ |
| Variance of fitting parameter n | $\sigma_n^2$ | - | 1.13x10$^{-2}$ |
| Coefficient of variation (k) | $CV(k)$ | - | 53.29 % |
| Coefficient of variation (α) | $CV(\alpha)$ | - | 10.03 % |
| Coefficient of variation (n) | $CV(n)$ | - | 7.86 % |
| Correlation length | $\eta_k$, $\eta_\alpha$, $\eta_n$ | m | 0.3 |
| Lower boundary water pressure | $P_w$ | Pa | 1.40x10$^5$ |
| Lower boundary oil pressure | $P_o$ | Pa | 1.55x10$^5$ |
| Upper boundary water flux | $Q_w$ | m/s | 1.0x10$^{-8}$ |
| Oil leakage rate | $F_o$ | kg/d | 100 |

**Table 2. Cases simulated in this study**

| Case | Conditioned Variables | Number of Measurements | Correlation Length (m) | Oil Source (kg/day) |
|---|---|---|---|---|
| Baseline | 0 | - | 0.3 | 100 |
| Case 1 | $Y, \beta, \overline{n}$ | 1 | 0.3 | 100 |
| Case 2 | $Y, \beta, \overline{n}$ | 4 | 0.3 | 100 |
| Baseline I | 0 | - | 0.3 | 10000 |
| Case 3 | $Y, \beta, \overline{n}$ | 1 | 0.3 | 10000 |
| Case 4 | $Y, \beta, \overline{n}$ | 4 | 0.3 | 10000 |
| Case 5 | $Y, \beta$ | 1 | 0.3 | 10000 |
| Case 6 | $Y, \overline{n}$ | 1 | 0.3 | 10000 |
| Case 7 | $\beta, \overline{n}$ | 1 | 0.3 | 10000 |
| Baseline II | 0 | - | 0.15 | 100 |
| Case 8 | $Y, \beta, \overline{n}$ | 1 | 0.15 | 100 |

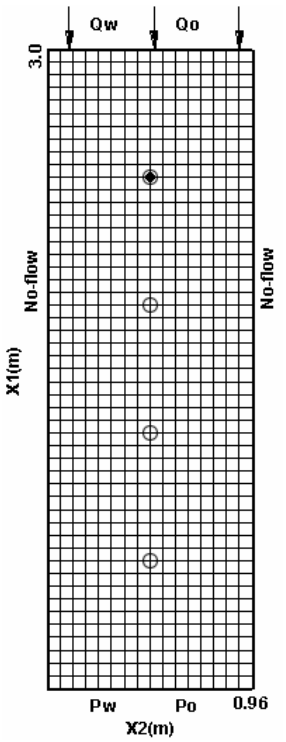


Fig. 1. Model domain

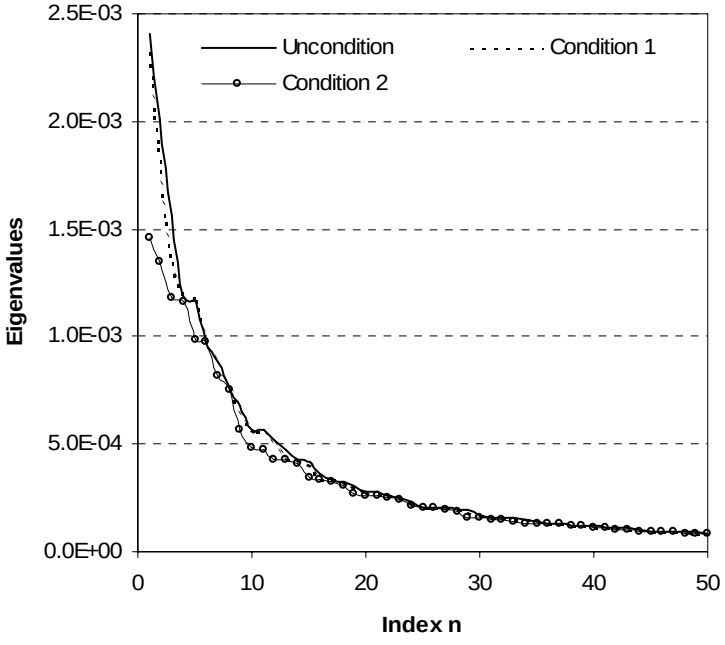


Fig. 2. Unconditional and conditional eigenvalues

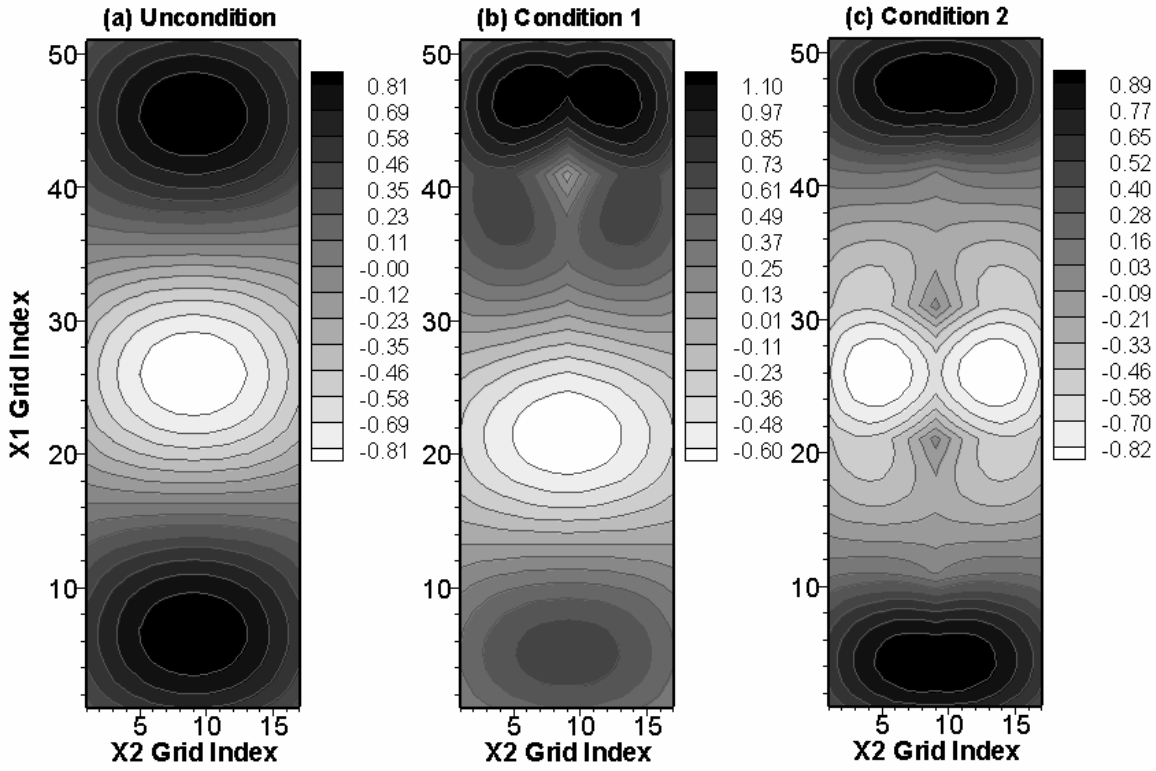


**Fig. 3. The third eigenfunctions (n=3) of (a) unconditional, (b) 1 measurement conditional, and (c) 4 measurement conditional simulations.**

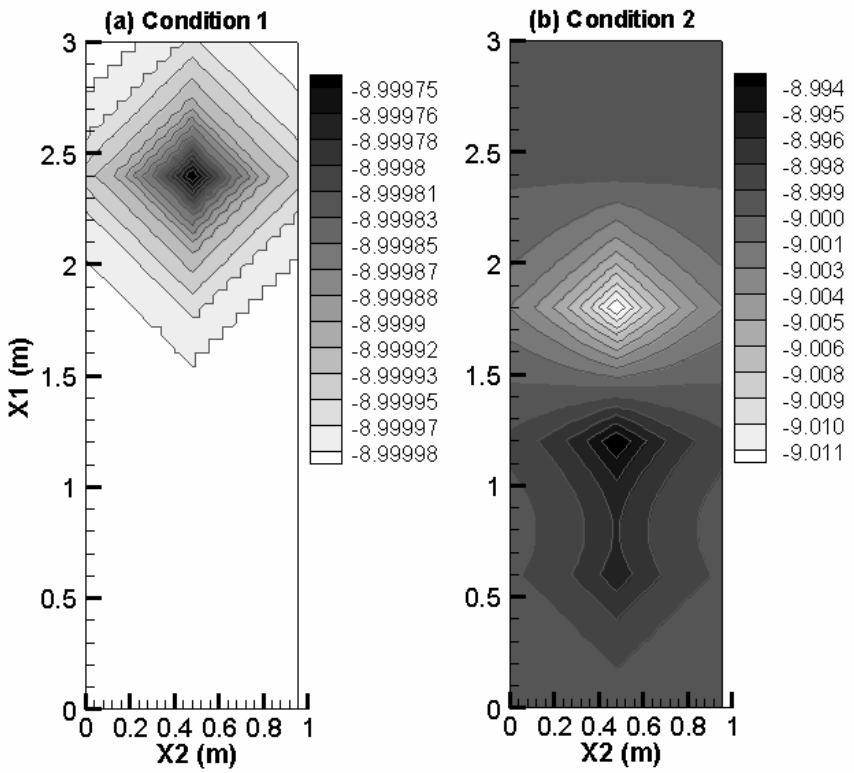


**Fig. 4. The means of log pore size distribution β with (a) 1 measurement, and (b) 4 measurements.**

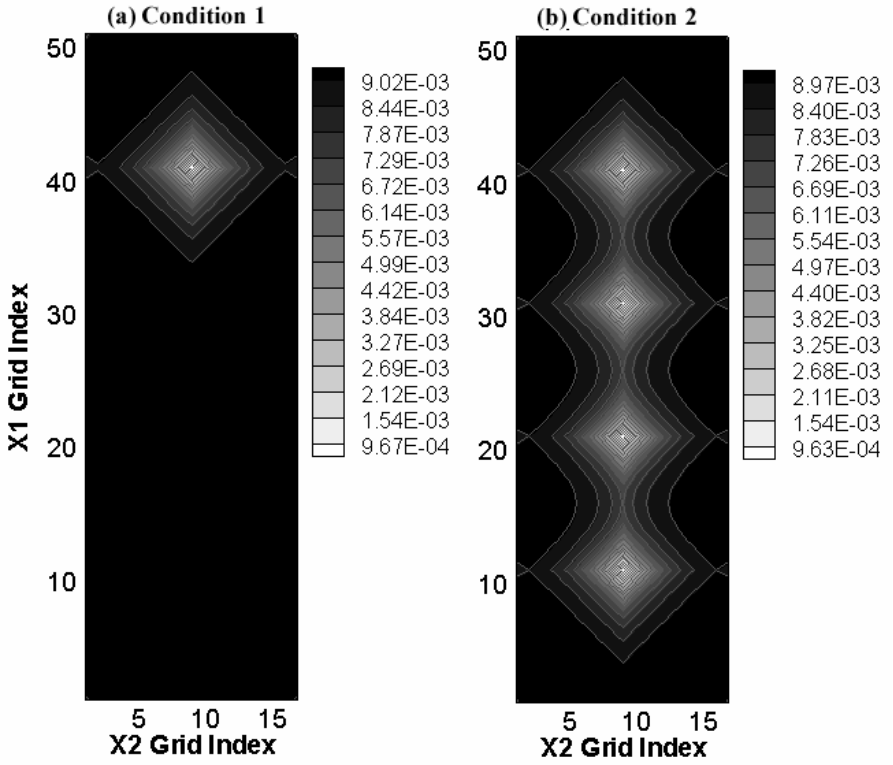


**Fig. 5. The variances of log pore size distribution β with (a) 1 measurement, and (b) 4 measurements.**

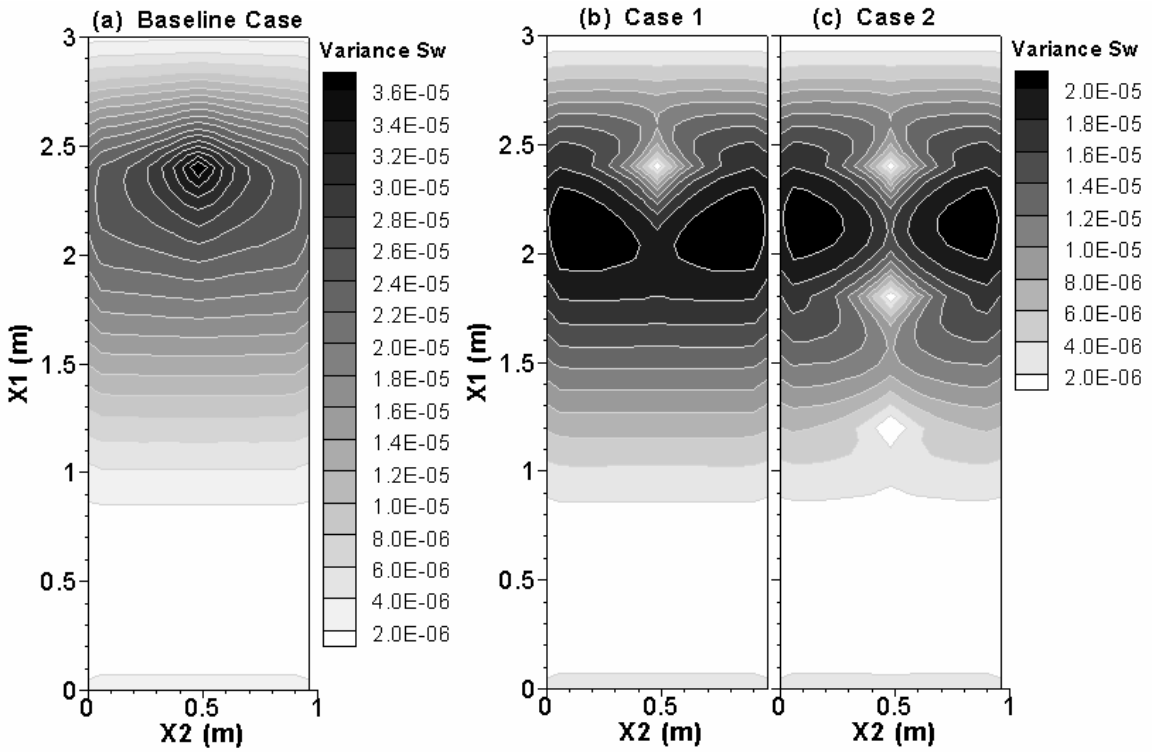


**Fig. 6. The contour map of variances of water saturation from (a) unconditional Baseline Case, (b) conditional Case 1 with one measurement, and (c) conditional Case 2 with four measurements.**

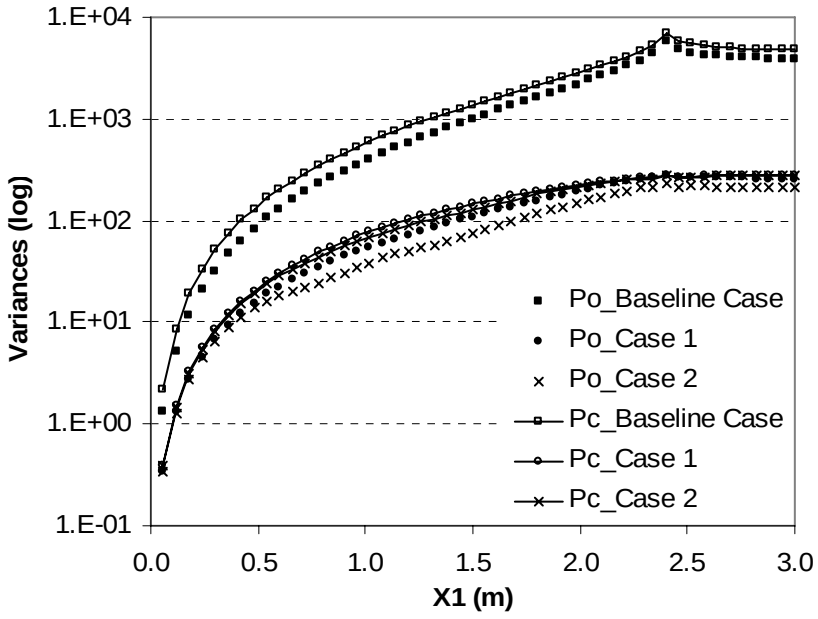


**Fig. 7. The variances along central vertical line (X2 = 0.48 m) of oil and capillary pressures from unconditional Baseline Case, conditional Case 1 and Case 2.**

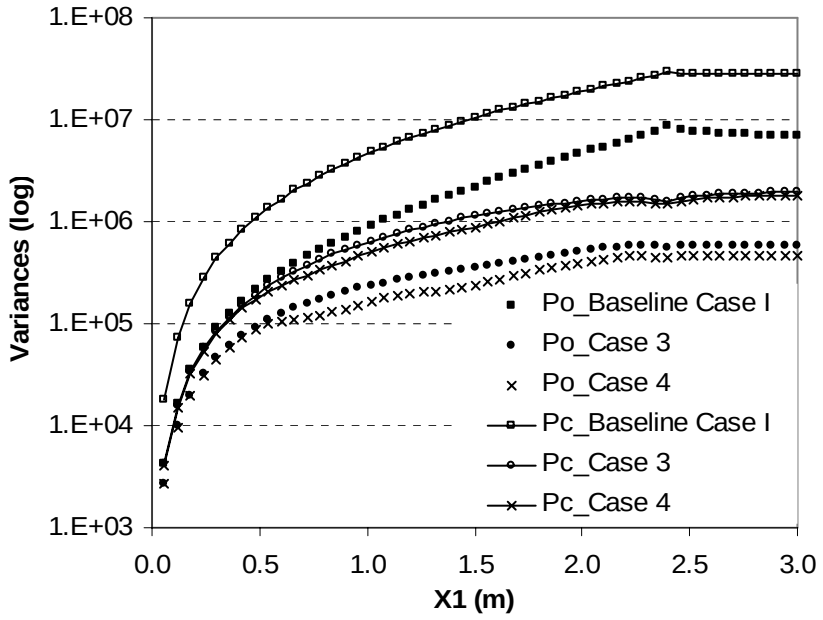


**Fig. 8. The comparison of variances along central vertical line (X2 = 0.48 m) of oil and capillary pressures between unconditional Baseline Case I, conditional Case 3 and Case 4.**

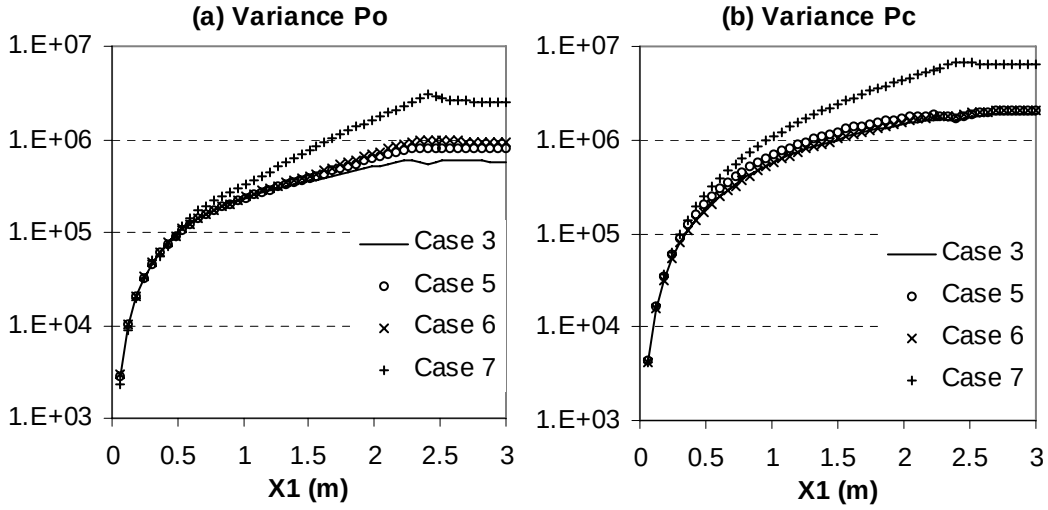


**Fig. 9. The comparison of variances along central vertical line (X2 = 0.48 m) between Case 4, Case 5, Case 6, and Case 7 for (a) oil pressure, and (b) capillary pressure.**

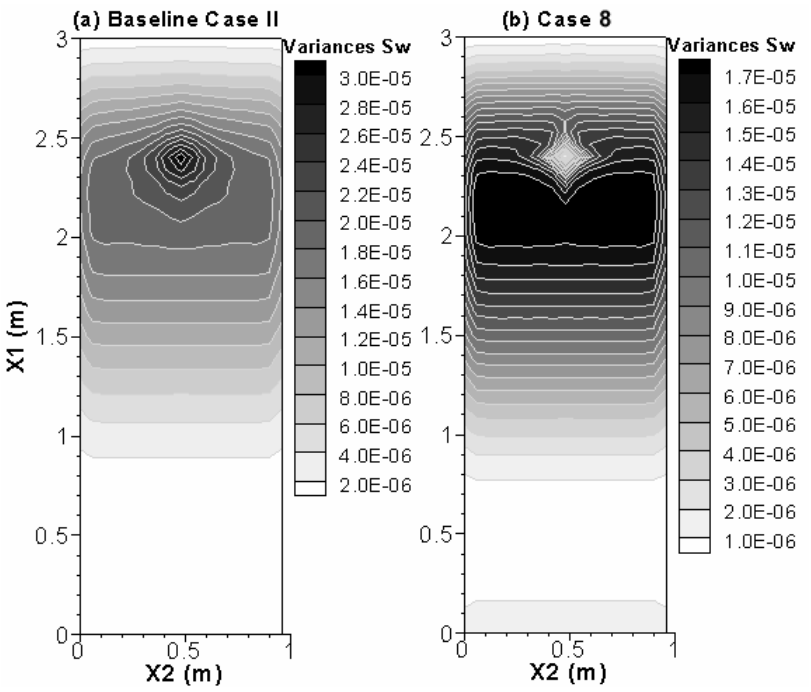


**Fig. 10. The contour map of variances of water saturation from (a) unconditional Baseline Case II, and (b) conditional Case 8.**

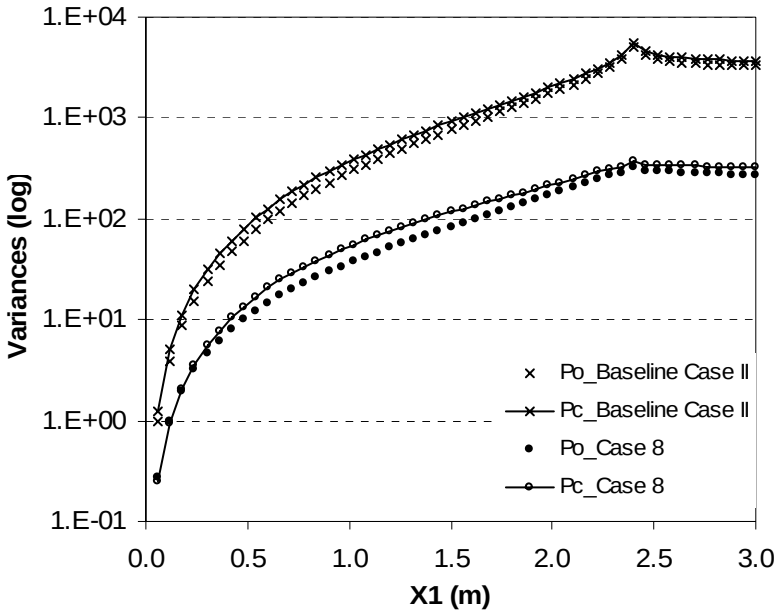


**Fig. 11. The variances along central vertical line (X2 = 0.48 m) of oil and capillary pressures from unconditional Baseline Case II, and conditional Case 8.**